ISSN 1063-7834, Physics of the Solid State, 2020, Vol. 62, No. 3, pp. 464–471. © Pleiades Publishing, Ltd., 2020.
Russian Text © The Author(s), 2020, published in Fizika Tverdogo Tela, 2020, Vol. 62, No. 3, pp. 413–420.

MAGNETISM

$HoFeTi_2O_7$: Synthesis, Peculiarities of the Crystal Structure, and Magnetic Properties

T. V. Drokina[a, *], M. S. Molokeev[a, b], D. A. Velikanov[a], G. A. Petrakovskii[a], and O. A. Bayukov[a]

[a] *Kirensky Institute of Physics, Krasnoyarsk Scientific Center, Siberian Branch, Russian Academy of Sciences, Krasnoyarsk, 660036 Russia*

[b] *Siberian Federal University, Krasnoyarsk, 660041 Russia*

**e-mail: tvd@iph.krasn.ru*

Received November 19, 2019; revised November 19, 2019; accepted November 19, 2019

Abstract—Polycrystalline samples of $HoFeTi_2O_7$ were obtained by solid-phase synthesis and investigated using X-ray diffraction, gamma resonance, and SQUID measurements. Characteristics of the structural properties are presented, which give an evidence of the distribution of iron atoms among nonequivalent crystallographic positions and of the nonuniform populating of positions mixed with titanium by the iron atoms. Spin disorder caused by mixing of magnetic and nonmagnetic ions, spatial nonuniformity of the interactions defining the magnetic structure in the crystal lead to formation of concurrent magnetic exchange interactions between the nearest neighbors, frustration of magnetic couplings, and loss of the long-range magnetic ordering. The temperature dependence of the magnetic susceptibility at low temperatures was shown to have some peculiarities typical of the magnetic state of spin glass.

Keywords: frustrated magnetics, crystal structure, spin disorder, static magnetic properties, spin glass

DOI: 10.1134/S1063783420030075

INTRODUCTION

Frustrated magnetic systems with different magnetic properties, capable of forming unusual ground magnetic states are widely studied today [1–5], which encourages seeking new magnetic materials. Compounds containing rare earth and transition 3*d* metals attract the attention of researchers in the field of solid-state physics [5–8]. Concurrent magnetic interactions are highly probable to appear in complex oxides based on 3*d* and 4*f* elements, which leads to frustration of magnetic moments.

The ground state of frustrated magnetics $R_2Ti_2O_7$ with the pyrochlore crystal structure (R is a rare earth ion) at low temperatures is a spin glass, like in $Dy_2Ti_2O_7$ or $Ho_2Ti_2O_7$ [3, 4]. The influence which substitution of certain ions in spin-frustrated magnetics has on their magnetic properties is of interest [5].

Compounds with the general composition $R^{3+}Fe^{3+}Ti_2O_7$ (R = Sm, Gd, Tb, Dy, Yb, Lu) possess the zirconolite crystal structure and are of a special interest due to the presence of two magnetic ions, which enriches the pattern of magnetic couplings in the crystal and lead to their concurrence in the spin system. The peculiarity of the zirconolite crystal structure with nonuniform distribution of iron ions over the mixed crystallographic positions facilitates formation of the magnetic spin-glass state [7–10]. These compounds can be used as model materials to understand the physics of disordered structures, micromagnetism, and for development of new types of magnetic memory devices.

The aim of this work is obtaining a new magnetic oxide compound of 3*d* and 4*f* elements with the formula $HoFeTi_2O_7$ and experimental studying its structural and magnetic properties. Holmium was chosen as the rare earth ion in the $RFe^{3+}Ti_2O_7$ system since it has one of the biggest magnetic moments among all elements on the periodic table.

EXPERIMENTAL

Polycrystalline sample of $HoFeTi_2O_7$ was obtained by solid-state synthesis in the mix of high-purity oxides Fe_2O_3, TiO_2, and Ho_2O_3 taken in the stoichiometric ratio. The samples were prepared as disks with the diameter of 10 mm and thickness of 1.5–2.0 mm and were subject to high-temperature treatment at 1200–1250°C in air. The synthesis procedure includes four annealing steps 24 h long each with intermediate wet grinding in alcohol. The chemical and phase composition of the obtained samples were controlled by X-ray structural analysis.

Powder X-ray diffraction pattern of $HoFeTi_2O_7$ was obtained at room temperature on a Bruker D8 ADVANCE diffractometer using a VANTEC linear detector and CuK_α radiation. Variable count time

(VCT) and variable step scanning (VSS) methods were used. The exposition time was increased as the 2θ angle grew to improve the quality of the acquired data [11–13]. As a rule, 5 to 8 experimental points should cover the peak half-width (FWHM). However, the peaks broaden significantly as the 2θ increase. Therefore, the step was wider for large 2θ values to decrease the duration of the experiments [14]. The experimental data were converted to a standard XYE file containing the coordinate $2\theta_i$, intensity I_i, and standard deviation $\delta(I_i)$ for each measured point. The Rietveld refinement that is implemented, e.g., in the TOPAS 4.2 software [15], allows for the standard deviation of each point by calculating the weight $w_i = 1/\sigma(I_i)^2$ for each point. Increasing the exposition time for a given point leads to a corresponding decrease in the standard deviation $\sigma(I_i)$ and an increase in its weight w_i in the least squares refinement procedure. Thus, the VCT method equilibrates the weights of weak large-angle and strong small-angle reflexes, in contrast to a conventional experiment where the weight are unequal and the structural information contained in the large-angle region is lost.

Nuclear gamma resonance spectra were recorded on a MS-1104Em spectrometer in the Kirensky Institute of Physics (Krasnoyarsk Scientific Center, Siberian Branch, Russian Academy of Sciences). Measurements were conducted at room temperature using a $Co_{57}(Cr)$ source in powders with the thickness of 5–10 mg/cm^2 at the natural iron abundance. The chemical shift values are given relative to α-Fe.

Temperature behavior of the magnetic moment was investigated on a Quantum design MPMS-XL magnetometer in the Siberian Federal University in the temperature range from 2 to 300 K using the following regimes: zero-field cooling (ZFC), when the sample was cooled to the liquid helium temperature without the magnetic field, then the measuring field $H = 500$ or 1000 Oe was turned on, the temperature began to rise, and the magnetic moment was measured, and in the field cooling mode (FC) when the magnetic moment was measured as the sample was cooled in the presence of the field H.

RESULTS AND DISCUSSION

Structural properties of polycrystalline compound $HoFeTi_2O_7$ were investigated by X-ray diffraction and nuclear gamma resonance.

The X-ray diffraction pattern of the synthesized $HoFeTi_2O_7$ sample at room temperature is shown in Fig. 1. The experimental diffraction pattern of the sample obtained following the VCT/VSS method was divided into four parts: 5°–38.7° (exposition time 3 s per one point, step 0.016°); 38.7°–61.6° (exposition 9 s, step 0.024°); 61.6°–97.5° (exposition 15 s, step 0.032°); and 97.5°–140° (exposition 24 s, step 0.040°). The total experiment time was 16 h. Partitioning of the experiment was made in the XRD Wizard program [14]. Peak positions were determined with the aid of the EVA program (2004 release) from the DIFFRAC-PLUS software package (Bruker).

Table 1. Basic crystallographic properties of $HoFeTi_2O_7$ and parameters of the X-ray experiment

	$HoFeTi_2O_7$
Space group	*Pcnb*
a, Å	9.8353(2)
b, Å	13.5572(2)
c, Å	7.3497(1)
V, Å^3	980.01(3)
Z	8
D_x, g/cm^3	5.796
μ, mm^{-1}	78.909
2θ range, deg	5–140
Number of reflexes	939
Number of refined parameters	82
R_{wp}, %	1.187
R_{exp}, %	0.915
R_p, %	1.657
GOF(χ)	2.063
R_{Bragg}, %	0.780

A small admixture (2.39%) of the phase Fe_2TiO_5 was noticed together with the main phase $HoFeTi_2O_7$. Note that the studied compound $HoFeTi_2O_7$ is isostructural to $GdGaTi_2O_7$ [16]. Thus, the structure of $GdGaTi_2O_7$ was taken as the initial model for the analysis of the crystal structure and determination of the position populations in the sample of $HoFeTi_2O_7$. Main crystallographic characteristics of $HoFeTi_2O_7$ and parameters of the X-ray experiment are listed in Table 1. Atom coordinates and results of refinement of the population of crystallographic positions of p atoms in $HoFeTi_2O_7$ are given in Table 2.

According the obtained X-ray data, the structure of the $HoFeTi_2O_7$ sample at room temperature is described by the centrosymmetrical rhombic syngony with the space group *Pcnb*, like other studied compounds with the general formula $RFeTi_2O_7$ (with the rare earth ion R = Sm, Gd, Tb, Dy, Yb, Lu) [8–10, 17, 18].

Crystal structure of the $RFeTi_2O_7$ compounds, as well as $GdGaTi_2O_7$, consists of four-, five-, six-, and eight-apical oxygen-coordinated polyhedra. The rare earth ion is placed in the eight-apical polyhedron. Iron occupies three close but inequivalent crystallographic positions; Fe^{3+} cations are placed in a distorted octahedron which can be presented conditionally as two

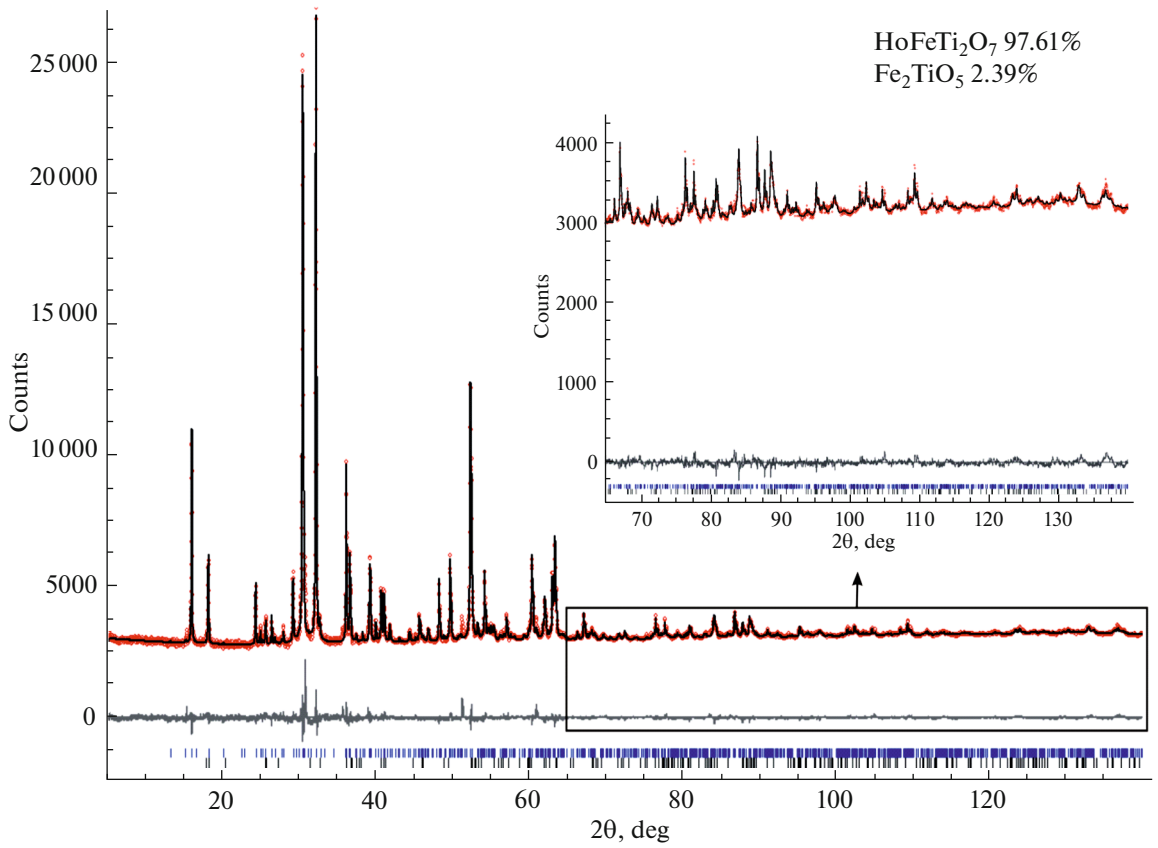

Fig. 1. X-ray diffraction of the polycrystalline sample of $HoFeTi_2O_7$ at room temperature. The bottom line is the difference plot. The studied compound contains the admixture of Fe_2TiO_5 at the level of 2.39%.

polyhedra: a tetrahedron with the Fe_t ion in the center and a coordination five-apical polyhedron with the Fe_f ions (Fe'_f,Fe''_f) [16]. Symmetry-related cations Fe'_f and Fe''_f are situated along the diagonal of the composite octahedron. In addition, polyhedra of mixed octahedral positions Ti–Fe(Ga) are also involved in building the crystal structure of the discussed compounds: Ti1–Fe1(Ga1), Ti2–Fe2(Ga2), and Ti3–Fe3(Ga3).

Analysis of the results shows that the lattice parameter a in $HoFeTi_2O_7$ is increased, while b and c are decreased as compared to the lattice parameters of $GdGaTi_2O_7$ (a = 9.7804(3) Å, b = 13.605(1) Å, c = 7.4186(2) Å [16]); that is, disproportional changes of the parameters of the rhombic cell occurs upon substituting holmium and iron cations for gadolinium and gallium cations. Moreover, populations of the mixed positions Fe–Ti in $HoFeTi_2O_7$ and Ga–Ti in $GdGaTi_2O_7$ also differ. Gallium occupies all three mixed positions in $GdGaTi_2O_7$; the populations are 0.12 for Ga1, 0.21 for Ga2, and 0.27 for Ga3 [16]. Table 2 shows that the mixed position Ti3–Fe3 is occupied by titanium ions in the holmium-containing sample.

Note that the X-ray studies reveal the following content of the elements in the unit cell of the synthesized $HoFeTi_2O_7$ sample: $0.89 \times 8 + 0.2 \times 4 + 1.00 \times 8 = 15.92$ titanium atoms and $0.11 \times 8 + 0.8 \times 4 + 0 \times 8 + (0.78 \times 4 + 0.11 \times 8) = 8.08$ iron atoms. The resulting formula allowing for the standard deviations can be written as $HoFe_{1.01(9)}Ti_{1.99(9)}O_7$.

Thus, distribution of iron ions among four (from five possible) crystallographic positions and unequal population of the mixed positions Ti1–Fe1 and Ti2–Fe2 by the iron ions is a peculiarity of the crystal structure of $HoFeTi_2O_7$ important in this study.

Additional information on the structure is given by Mössbauer spectroscopy. Absorption spectrum by ^{57}Fe nuclei in $HoFeTi_2O_7$ at 300 K is shown in Fig. 2a. The horizontal axis shows the relative speed of the source relative to the absorber, the vertical axis presents the intensity of resonance absorption. The γ quanta absorption spectrum by ^{57}Fe nuclei in the $HoFeTi_2O_7$ sample is a sum of overlapping quadrupole doublets.

To determine the composition of the model spectrum, the probability distribution of quadrupole splittings P(QS) in the experimental spectrum was calcu-

Table 2. Atom coordinates, populations of the structure positions p in the $HoFeTi_2O_7$ crystal, and thermal factors B_{iso}

Atom	Population of the position	x	y	z	p	B^*_{iso}/B_{eq}
Ho	8	0.2447 (5)	0.1321 (3)	0.0072 (6)	1	1.47 (10)
Ti1	8	0.2439 (12)	0.3855 (6)	0.4797 (10)	0.892 (42)	1.24 (18)
Fe1	8	0.2439 (12)	0.3855 (6)	0.4797 (10)	0.108 (42)	1.24 (18)
Ti2	4	0.5	0.25	0.249 (3)	0.21 (18)	1.8 (4)
Fe2	4	0.5	0.25	0.249 (3)	0.79 (18)	1.8 (4)
Ti3	8	0.0025 (11)	0.4891 (6)	0.253 (2)	1.00 (10)	2.1 (3)
Fe3	8	0.0025 (11)	0.4891 (6)	0.253 (2)	0.00 (10)	2.1 (3)
Fet	4	0	0.25	0.338 (3)	0.78	3.77 (3)
Fef	8	0.041 (8)	0.274 (6)	0.173 (12)	0.11	3.77 (3)
O1	8	0.1617 (12)	0.3871 (16)	0.242 (4)	1	1.20 (18)
O2	8	0.4142 (17)	0.1098 (17)	0.254 (5)	1	1.20 (18)
O3	8	0.112 (2)	0.1472 (12)	0.251 (5)	1	1.20 (18)
O4	8	0.386 (4)	0.280 (2)	0.448 (4)	1	1.20 (18)
O5	8	0.369 (3)	0.289 (3)	0.046 (4)	1	1.20 (18)
O6	8	0.369 (3)	0.497 (2)	0.430 (4)	1	1.20 (18)
O7	8	0.379 (4)	0.482 (2)	0.070 (4)	1	1.20 (18)

Table 3. Mössbauer parameters of $HoFeTi_2O_7$

IS, mm/s ±0.01	QS, mm/s, ±0.02	W, mm/s ±0.02	$A(\gamma)$, partial % ±0.04	A(R)	EFG, e/Å^3	Position
0.24	2.19	0.26	0.21	0.114	−0.247	Fe_f
0.23	2.36	0.19	0.10	0.101	0.501	Fe_t
0.35	0.59	0.26	0.18	0.168	0.190	Fe_1
0.35	0.86	0.32	0.31	0.616	−0.173	Fe2
0.30	1.43	0.56	0.21			“Fe2”

lated and presented in Fig. 2b. Two groups of doublets with different chemical shifts were used in the calculation of P(QS). The doublet amplitudes and chemical shifts common for each doublet group were fitted. The chemical shift values obtained as the result of the fitting are shown as numbers in Fig. 2b. A small value IS = 0.23 mm/s proves that this doublet group is related to Fe^{3+} cations with a low oxygen coordination. The doublet group with IS = 0.35 mm/s belongs to the Fe^{3+} cations occupying the octahedral positions. Maxima and peculiarities on the P(QS) distribution curve give an evidence of nonequivalent positions of iron in $HoFeTi_2O_7$.

Information extracted from the P(QS) distribution was used to simulate a model spectrum and fit it to the experimental one by varying the whole set of hyperfine parameters. The fitting results for $HoFeTi_2O_7$ are given in Table 3, where IS is the isomeric shift relative to α-Fe, QS is the quadrupole splitting, W is the absorption line width, and $A(\gamma)$ is the partial population of the position (the area under the partial doublet). All components of the Mössbauer spectrum are shown in Fig. 2a by the lines. The error spectrum (difference of the calculated and experimental spectra) is plotted under the experimental spectrum.

To identify the Mössbauer positions of iron in zirconolite $HoFeTi_2O_7$ (assignment to the crystallographic positions), the X-ray diffraction results were used, namely, iron populations at the positions and the distortion degree of the coordination polyhedra. The EFG column in Table 3 shows the estimate of the electric field gradient (EFG) created by the anions in the coordination polyhedra at the crystallographic positions of the iron atoms. With this goal, we used X-ray data on the coordinates of atoms that form the $HoFeTi_2O_7$ lattice. EFG values should correlate with experimental quadrupole splittings QS. No such correlation is observed. There may be two reasons for this discrepancy. First, the contribution of the far neighbors was not taken into account when estimating the

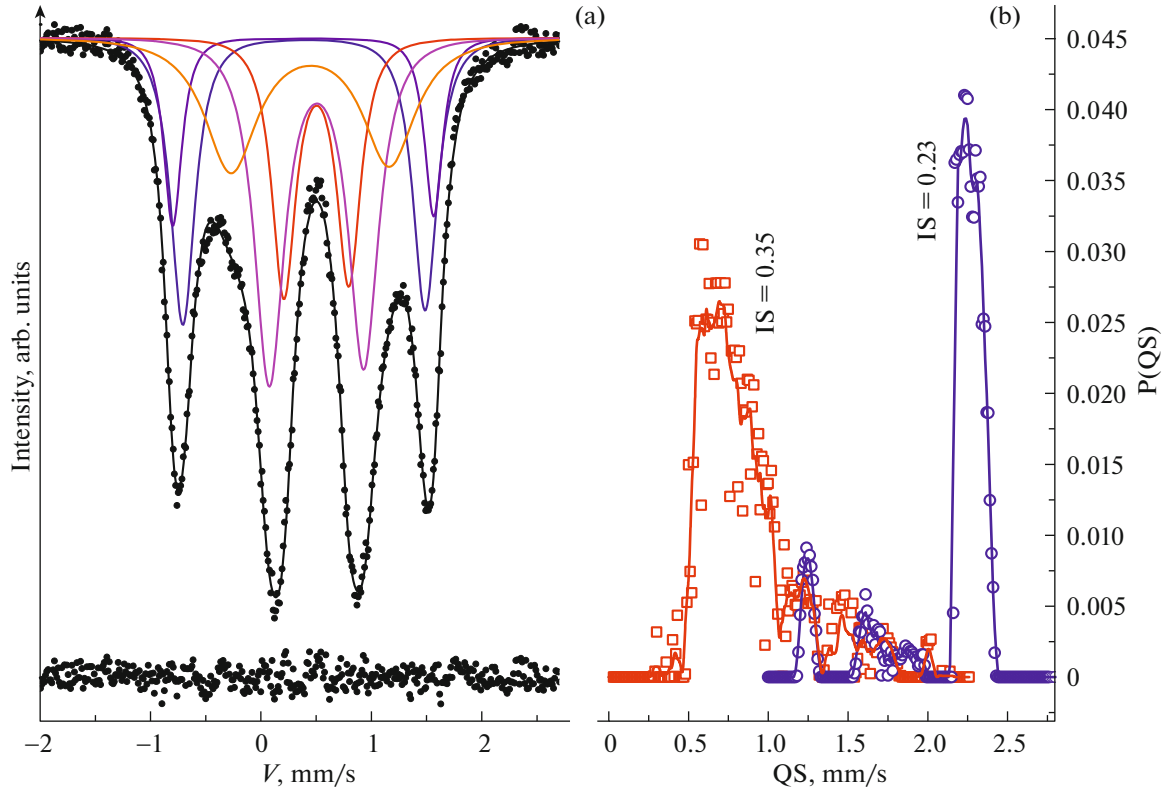

Fig. 2. (a) Mössbauer spectrum of $HoFeTi_2O_7$ at $T = 300$ K. (b) Distribution of the quadrupole splitting probability in the experimental spectrum of $HoFeTi_2O_7$.

EFG. Second, X-ray analysis does not distinguish between local environments of Fe and Ti in the mixed positions, giving atom coordinates that are averaged over the lattice. The electric field gradient (and, hence, quadrupole splitting) is, however, quite sensitive to small variations of the atom coordinates.

The columns $A(\gamma)$ and $A(R)$ in Table 3 give the position populations measured by the Mössbauer and X-ray methods, respectively. The results agree with each other on the qualitative level, which allowed us to identify the Mössbauer positions. Appearance of the position Fe_f is probably due to iron cations contained in the admixture Fe_2TiO_5 [19, 20].

Note that the gamma resonance investigation proves that the character of the Mössbauer spectrum is consistent with the idea of the presence of nonequivalent iron ion positions in the crystal lattice of the dielectric compound $HoFeTi_2O_7$.

Thus, the results of X-ray and Mössbauer investigations show chaotic distribution of iron atoms over the crystallographic positions in $HoFeTi_2O_7$: atoms of iron and titanium are randomly distributed among the mixed Ti–Fe centers of the crystal lattice.

The magnetic subsystem of the $HoFeTi_2O_7$ sample is formed by iron and holmium ions. Titanium ions in the multiatomic crystal $HoFeTi_2O_7$ are in the diamagnetic state $Ti^{4+}(3d^0)$. Magnetic properties of oxide compounds synthesized from the transition $3d$ element (Fe) and $4f$ elements (rare earths) depend strongly on the features of their electron configurations. In $HoFeTi_2O_7$ magnetic ions Fe^{3+} have the electron configuration $3d^5$, and Ho^{3+} ions have the configuration $4f^{10}5s^25p^65d^16s^2$. Closed outer shells ($5s^25p^6$) shield the magnetic $4f$ shell of the rare earth Ho^{3+} ion from the influence of neighbor atoms. Unlike Ho^{3+}, the empty d shell of the iron ions is closer to the shell periphery and thus more prone to external influence in the crystal.

Measurements of the temperature and field dependences of the magnetic moment were carried out to analyze magnetic properties of $HoFeTi_2O_7$ (Figs. 3, 4).

It is evident from Fig. 3a that the temperature dependence of the magnetic moment $M(T)$ (in the ZFC measuring mode) in the field of $H = 500$ Oe has a maximum at 3.8 K. Curves $M(T)$ obtained in the ZFC and FC modes are plotted in Fig. 3b; the magnetic moments are different to the temperature of $T_f = 4.7$ K, and coincide above the T_f point. This kind of the temperature dependence of the magnetic moment, which demonstrates the influence of the prehistory (namely, on cooling conditions: in the field and with the field turned on only after cooling to the tempera-

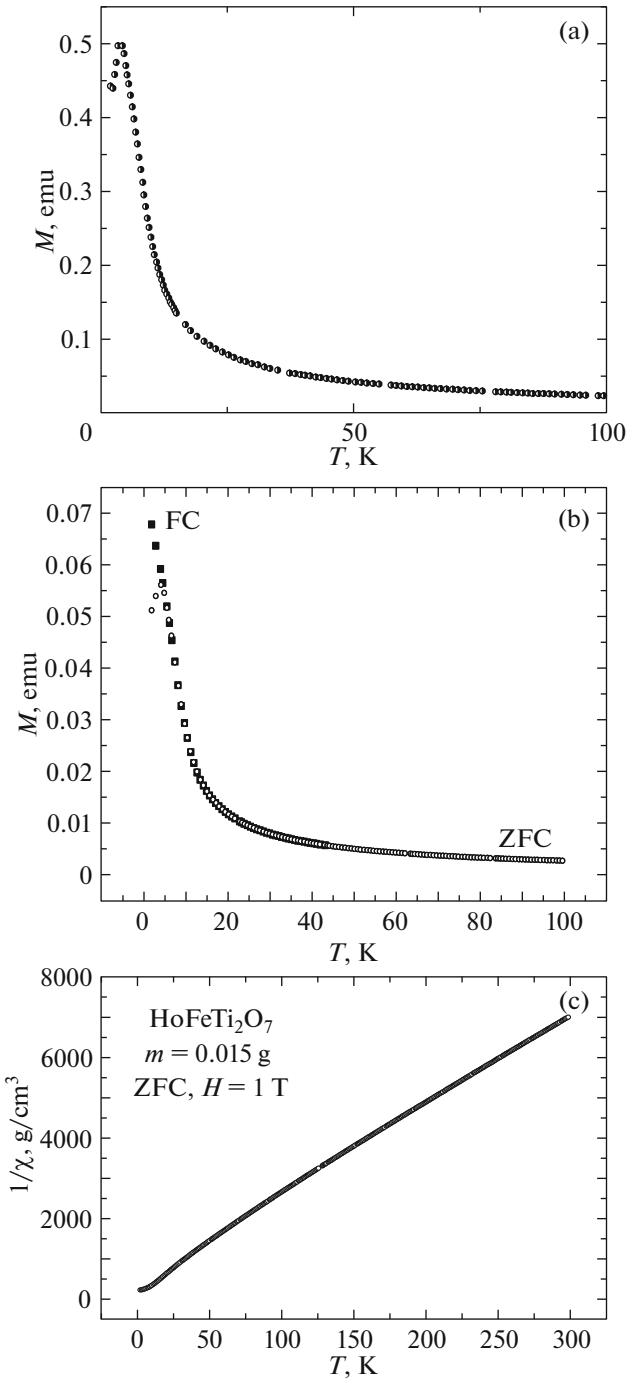

Fig. 3. (a) Temperature dependence of the magnetic moment of the $HoFeTi_2O_7$ sample in the field of H = 0.05 T. Sample was cooled in the zero field. The sample mass was m = 0.145 g. (b) Dependence of the magnetic moment of the $HoFeTi_2O_7$ sample on the temperature in the field of 0.05 T obtained in two measurement modes: FC (sample was cooled at H = 0.05 T) and ZFC (H = 0). The sample mass was m = 0.015 g. The freezing temperature was T_f = 4.7 K. (c) Temperature dependence of the inverse susceptibility of the $HoFeTi_2O_7$ sample cooled without the magnetic field. The asymptotic Neel temperature is $\theta = -28$ K. The sample mass was m = 0.015 g.

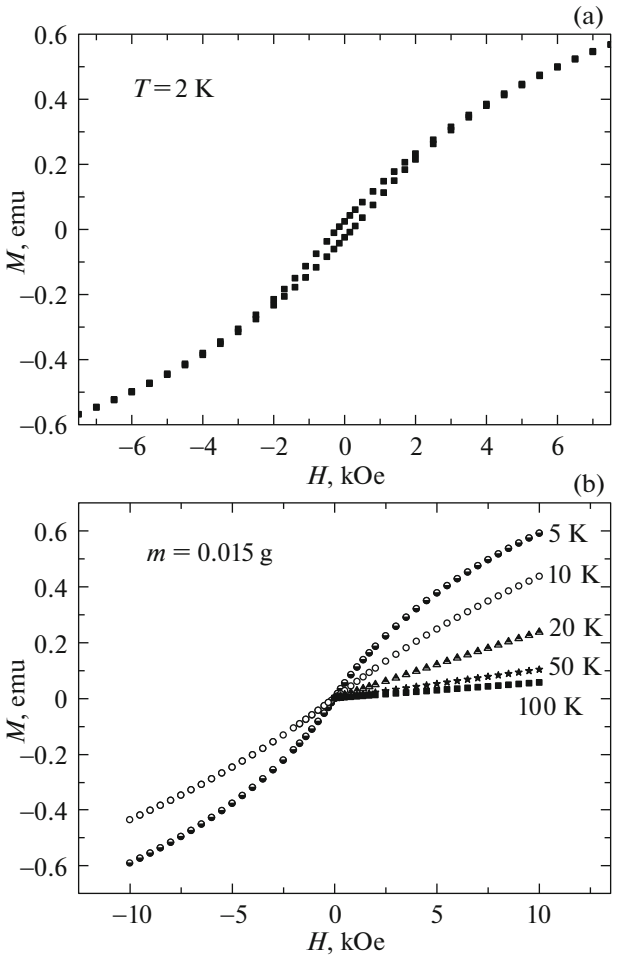

Fig. 4. (a) Magnetic hysteresis loop in $HoFeTi_2O_7$ at T = 2 K. The coercive force was H_c = 225 Oe. The sample mass was m = 0.015 g. (b) Field dependences of the magnetic moment in $HoFeTi_2O_7$ at different temperatures. The sample mass was m = 0.015 g.

ture below T_f) is typical of a thermodynamically nonequilibrium metastable magnetic state of spin glass; it was observed earlier in compounds of the $RFeTi_2O_7$ class (R = Sm, Gd, Tb, Dy, Yb, Lu) [8–10, 17, 18].

Structural studies showed that iron atoms do not form a regular crystal lattice in the $HoFeTi_2O_7$ crystal, but rather are randomly distributed; this is one of the conditions of appearing of the magnetic spin glass state in a material. Peculiarities of the magnetic properties and the disorder in the distribution of magnetic iron ions in the crystal lattice allow suggesting that the magnetic spin glass state arises in $HoFeTi_2O_7$ below the "freezing" temperature T_f = 4.7 K.

Above the "freezing" point the studied material goes to the paramagnetic phase. The temperature dependence of the inverse susceptibility $\chi^{-1}(T)$ in the temperature range of 2–300 K with the $HoFeTi_2O_7$ sample cooled in the magnetic field of H = 1000 Oe is

plotted in Fig. 3c. The dependence of the inverse susceptibility in the high-temperature range ($T > 75$ K) obeys the Curie–Weiss law $\chi = C/(T - \theta)$, where C is the Curie–Weiss constant and θ is the asymptotic Neel temperature.

According to the Curie–Weiss law, the paramagnetic state in $HoFeTi_2O_7$, in which the energy of thermal excitation is larger than the energy of magnetic interactions, is characterized by a negative asymptotic Neel temperature $\theta = -28$ K. This indicated that the interaction in the magnetic subsystem of the complex oxide compound of holmium and iron is mainly of the antiferromagnetic type. Table 4 shows main magnetic properties of the sample: experimental values of the asymptotic Neel temperature, Curie–Weiss constants, calculated and experimental effective moments for the temperature range in which the susceptibility obeys the Curie–Weiss law. The effective magnetic moment per a single molecule $\mu_{eff(exp)}$, derived from the experimental data, is comparable with the calculated value $\mu_{eff(calc)}$.

The main contribution into the magnetic moment of $HoFeTi_2O_7$ belongs to the holmium ions. The magnetic moment of the trivalent Ho^{3+} ion is $\mu_{eff} = 10.5\mu_B$; of the Fe^{3+} ion, $\mu_{eff} = 5.9\mu_B$ [21]. Despite the weaker contribution of the iron ions into the magnetic moment of the compound $HoFeTi_2O_7$, replacement of the rare earth ion R^{3+} in the system $RFeTi_2O_7$ by holmium does not change the ground magnetic state. The magnetic sublattice of iron was shown in [8] to play the key role in formation of a spin glass magnetic state in the system $RFeTi_2O_7$. This conclusion is also proven by the finding of the spin glass state in the holmium-containing sample, while holmium has one of the largest magnetic moments among all rare earth ions.

Figure 4 illustrates the behavior of the sample in the magnetic field. Hysteresis loop in $HoFeTi_2O_7$ obtained at $T = 2$ K is shown in Fig. 4a. The coercive force H_c was found to be 225 Oe. Figure 4b shows isotherms of the field dependence of the magnetic moment, characterizing the paramagnetic phase of the $HoFeTi_2O_7$ sample.

Since the exchange interaction energy depends on the disposition of magnetic and nonmagnetic ions, the random distribution of the iron ions in the lattice of $HoFeTi_2O_7$, on the one hand, and the presence of the second magnetic ion—holmium—on the other hand, may lead to the situation when the exchange interaction energy will change stochastically its value and even the sign depending on the distances between atoms in the magnetic subsystem. Not only changes in the positions of magnetic atoms of Fe and Ho are important here, but also of nonmagnetic Ti atoms. Anisotropy can also vary in a random way, in addition to the exchange, due to this disorder. Fluctuations of the inner electric field acting on the electrons of the d and f shells may result in the fluctuations of the energy of single-ion anisotropy and of the direction of the anisotropy axis [22]. Spin disorder arising due to mixing of magnetic and nonmagnetic ions changes in the interactions defining the magnetic structure in the crystal facilitate the formation of concurrent magnetic exchange interactions between the nearest neighbors and frustration of magnetic couplings. Estimate of the frustration level F by the relation $F = |\theta|/T_f$ [23] in the magnetic compound $HoFeTi_2O_7$ yields the value of 6.2.

Table 4. Asymptotic Neel temperatures θ, Curie–Weiss constants C in the Curie–Weiss law, calculated and experimental values of the effective moment for $HoFeTi_2O_7$

Compound	$HoFeTi_2O_7$
Freezing temperature T_f, K	4.5
Asymptotic Neel temperature θ, K	−28
Curie–Weiss constant C, K	0.047
$\mu_{eff(calc)} = (\mu_1^2 + \mu_2^2)^{1/2}$, where $\mu_i = g_i[J_i(J_i + 1)]^{1/2}$, μ_B	12.1
$\mu_{eff(exp)}$, μ_B	12.8

The effective moment of the compound was calculated as $\mu_{eff(calc)} = (\mu_1^2 + \mu_2^2)^{1/2}$, where the resulting moments of the iron ions Fe^{3+} ($i = 1$) and the rare earth metal R^{3+} ($i = 2$) $\mu_i = g_i(J_i(J_i + 1))^{1/2}$, μ_B (J_i is the total angular momentum and g_i is the spectroscopic splitting factor).

Thus, peculiarities of the crystal structure of zirconolite leading to a disorder in the disposition of the magnetic iron ions, and their mixing with nonmagnetic titanium ions in the centers of the crystal lattice lead to formation of a magnetic spin glass state in $HoFeTi_2O_7$ at low temperatures.

CONCLUSIONS

Properties of a novel magnetic compound $HoFeTi_2O_7$ were investigated by X-ray and gamma resonance methods and measurements of static magnetic characteristics.

The crystal structure of the sample is described by the rhombic space group *Pcnb* with the following unit cell parameters: $a = 9.8353(2)$ Å, $b = 13.5572(2)$ Å, $c = 7.3497(1)$ Å, $V = 980.01(3)$ Å^3. The crystallochemical formula of the studied compound, allowing for the relative populations of the individual position, is $HoFe_{1.01(9)}Ti_{1.99(9)}O_7$.

Analysis of X-ray diffraction and Mössbauer spectroscopy results showed the presence of a disordered distribution of iron ions in the crystal lattice of $HoFeTi_2O_7$.

The ground magnetic state, formed due to magnetic interactions between the Ho^{3+} and Fe^{3+} ions in $HoFeTi_2O_7$ with predominantly antiferromagnetic character in the magnetic subsystem, is subject to the

influence of fluctuations resulting from the stochastic distribution of the iron magnetic moments over the crystallographic positions mixed with nonmagnetic titanium ions. When the temperature decreases below 4.7 K, the $HoFeTi_2O_7$ sample with a complex pattern of spatially nonuniform concurrent magnetic interactions between the nearest neighbors experience a transition from the paramagnetic phase to a state with an typical indication of the spin glass: the magnetization depends not only on the temperature but also on the cooling conditions (in the external magnetic field and without the field).

Disordered distribution of the iron ions in the crystal lattice of $HoFeTi_2O_7$ facilitates arising of concurrent magnetic interactions, their frustration, absence of the long-range magnetic order, and the magnetic spin glass state appearing at low temperatures.

CONFLICT OF INTERESTS

The authors claim they have no conflicts of interest.

REFERENCES

1. S. S. Sosin, L. A. Prozorova, and A. I. Smirnov, Phys. Usp. **48**, 83 (2005).
2. M. Iakovleva, E. Vavilova, H.-J. Grafe, S. Zimmermann, A. Alfonsov, H. Luetkens, H.-H. Klauss, A. Maljuk, S. Wurmehl, B. Buchner, and V. Kataev, Phys. Rev. B **91**, 144419 (2015).
3. O. A. Petrenko, M. R. Lees, and G. Balakrishnan, Phys. Rev. B **68**, 012406 (2003).
4. S. Erfanifam, S. Zherlitsyn, J. Wosnitza, R. Moessner, O. A. Petrenko, G. Balakrishnan, and A. A. Zvyagin, Phys. Rev. B **84**, 220404(R) (2011).
5. H. Liu, Y. Zou, L. Ling, L. Zhang, W. Tong, C. Zhang, and Y. Zhang, J. Magn. Magn. Mater. **369**, 107 (2014).
6. V. V. Kucheryaev, E. I. Kunitsyna, R. A. Valeev, D. V. Korolev, V. P. Piskorskii, and R. B. Morgunov, Phys. Solid State **60**, 2481 (2018).
7. T. Drokina, G. Petrakovskii, M. Molokeev, A. Arauzo, and J. Bartolome, Phys. Proc. **12**, 580 (2015).
8. T. Drokina, G. Petrakovskii, M. Molokeev, J. Bartolomé, and A. Arauzo, J. Magn. Magn. Mater. **440**, 41 (2017).
9. G. A. Petrakovskii, T. V. Drokina, A. L. Shadrina, D. A. Velikanov, O. A. Bayukov, M. S. Molokeev, A. V. Kartashev, and G. N. Stepanov, Phys. Solid State **53**, 1855 (2011).
10. T. V. Drokina, G. A. Petrakovskii, M. S. Molokeev, D. A. Velikanov, O. N. Pletnev, and O. A. Bayukov, Phys. Solid State **55**, 2037 (2013).
11. I. C. Madsen and R. J. Hill, Adv. X-ray Anal. **35**, 39 (1992).
12. I. C. Madsen and R. J. Hill, J. Appl. Crystallogr. **27**, 385 (1994).
13. W. I. F. David, Abstract P2.6; NIST Spec. Publ. **846**, 210 (1992).
14. *Diffrac-Plus Basic XRD Wizard* (Bruker AXS, Karlsruhe, Germany, 2002–2007).
15. Bruker AXS, *TOPAS V4: General Profile and Structure Analysis Software for Powder Diffraction Data, User's Manual* (Bruker AXS, Karlsruhe, Germany, 2008).
16. E. A. Genkina, V. I. Andrianov, E. L. Belokoneva, B. V. Mill', B. A. Maksimov, and R. A. Tamazyan, Sov. Phys. Crystallogr. **36**, 796 (1991).
17. T. V. Drokina, G. A. Petrakovskii, M. S. Molokeev, and D. A. Velikanov, Phys. Solid State **60**, 532 (2018).
18. G. A. Petrakovskii, T. V. Drokina, D. A. Velikanov, O. A. Bayukov, M. S. Molokeev, A. V. Kartashev, A. L. Shadrina, and A. A. Mitsuk, Phys. Solid State **54**, 1813 (2012).
19. W. Q. Guo, S. Malus, D. H. Ryan, and Z. Altounian, J. Phys.: Condens. Matter **11**, 6337 (1999).
20. G. Seitz, N. Penin, L. Decoux, A. Wattiaux, M. Duttine, and M. Gaudon, Inorg. Chem. **55**, 2499 (2016).
21. K. P. Belov, M. A. Belyanchikova, R. Z. Levitin, and S. A. Nikitin, *Rare Earth Ferro and Antiferromagnets* (Nauka, Moscow, 1965) [in Russian].
22. I. Ya. Korenblit and K. F. Shender, Sov. Phys. Usp. **32**, 139 (1989).
23. J. A. Mydosh, *Spin-Glasses: An Experimental Introduction* (Taylor and Francis, London, 1993).

Translated by S. Efimov